Earth and Planetary Science Letters xxx (2008) xxx–xxx

Contents lists available at ScienceDirect

Earth and Planetary Science Letters

journal homepage: www.elsevier.com/locate/epsl

Mercury's internal magnetic field: Constraints on large- and small-scale fields of crustal origin

Michael E. Purucker [a,*], Terence J. Sabaka [a], Sean C. Solomon [b], Brian J. Anderson [c], Haje Korth [c], Maria T. Zuber [d], Gregory A. Neumann [e]

[a] Raytheon at Planetary Geodynamics Laboratory, Code 698, NASA Goddard Space Flight Center, Greenbelt, MD 20771, USA
[b] Department of Terrestrial Magnetism, Carnegie Institution of Washington, Washington, D.C. 20015, USA
[c] Johns Hopkins University Applied Physics Laboratory, 11100 Johns Hopkins Road, Laurel, MD 20723, USA
[d] Department of Earth, Atmospheric, and Planetary Sciences, Massachusetts Institute of Technology, Cambridge, MA 02139, USA
[e] Planetary Geodynamics Laboratory, Code 698, NASA Goddard Space Flight Center, Greenbelt, MD 20771, USA

A R T I C L E I N F O

Article history:
Accepted 9 December 2008
Available online xxxx

Editor: T. Spohn

Keywords:
Mercury
magnetic field
planetary magnetism

A B S T R A C T

MESSENGER and Mariner 10 observations of Mercury's magnetic field suggest that small-scale crustal magnetic fields, if they exist, are at the limit of resolution. Large-scale crustal magnetic fields have also been suggested to exist at Mercury, originating from a relic of an internal dipole whose symmetry has been broken by latitudinal and longitudinal variations in surface temperature. If this large-scale magnetization is confined to a layer averaging 50 km in thickness, it must be magnetized with an intensity of at least 2.9 A/m. Fits to models constrained by such large-scale insolation variations do not reveal the predicted signal, and the absence of small-scale features attributable to remanence further weakens the case for large-scale magnetization. Our tests are hindered by the limited coverage to date and difficulty in isolating the internal magnetic field. We conclude that the case for large- and small-scale remanence on Mercury is weak, but further measurements by MESSENGER can decide the issue unequivocally. Across the terrestrial planets and the Moon, magnetization contrast and iron abundance in the crust show a positive correlation. This correlation suggests that crustal iron content plays a determining role in the strength of crustal magnetization.

1. Introduction

Mercury's magnetic field was discovered by the Mariner 10 spacecraft during two flybys of the planet in 1974 and 1975. The dominantly dipolar internal magnetic field is oriented in the same sense as the Earth's, but its strength is only 1% as large. A quadrupolar component was suggested by the observations, but its magnitude was poorly constrained because of the limited spatial coverage of the planet afforded by the flybys (Connerney and Ness, 1988).

Magnetometer observations during the recent Mercury flyby by the MErcury Surface, Space ENvironment, GEochemistry, and Ranging (MESSENGER) spacecraft have been explained (Anderson et al., 2008) in terms of an internal dipole, magnetopause and tail currents, and large- and small-scale diamagnetic (plasma pressure) effects. These interpretations are supported by proton plasma count rates (Zurbuchen et al., 2008) and simulations of Mercury's magnetosphere (Trávníček et al., 2007).

By analogy with the Earth, the origin of Mercury's dipolar field could be a thermo-chemical dynamo in the planet's fluid outer core (Zuber et al., 2007). It has also been suggested that it might originate as the remanent of a dipole field, either through variations in the thickness of a coherently magnetized remanent layer (Aharonson et al., 2004) or in a layer of uniform thickness but relatively low magnetic permeability (Stephenson, 1976; Merrill, 1981; M. H. Acuña, personal communication, 2008). This paper will explore the constraints placed on small- and large-scale remanence by the three flybys, especially the recent MESSENGER flyby. A companion paper in this volume (Uno et al., 2008-this issue) explores the constraints placed on the origin of the field if it is the product of a core dynamo.

2. Data and modeling techniques

2.1. Magnetometer observations

A triaxial fluxgate Magnetometer (Anderson et al., 2007) mounted on a 3.6-m-long boom measured the magnetic field during MESSENGER's first Mercury flyby at a rate of 20 samples per second. The calibrated magnitude and three orthogonal magnetic field components are shown in Fig. 1 in a spherical Mercury-fixed coordinate

* Corresponding author. Tel.: +1 301 614 6473.
E-mail address: michael.e.purucker@nasa.gov (M.E. Purucker).

0012-821X/$ – see front matter © 2008 Published by Elsevier B.V.
doi:10.1016/j.epsl.2008.12.017

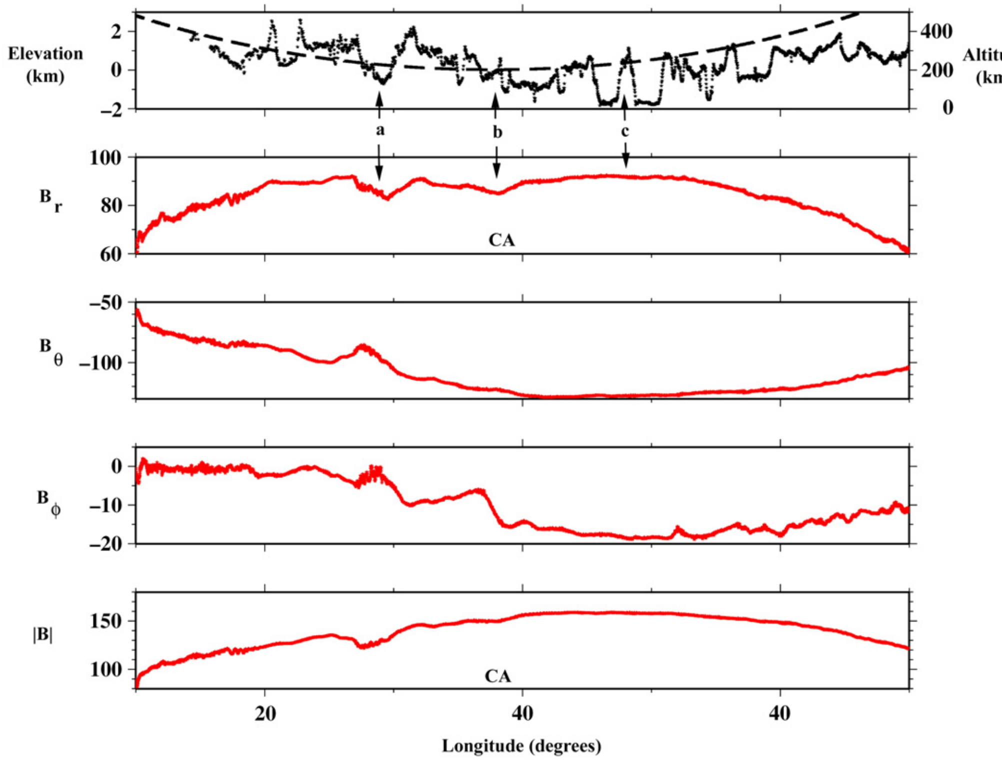

Fig. 1. Collocated Magnetometer and Mercury Laser Altimeter observations during the MESSENGER flyby of 14 January 2008. The uppermost record shows the MLA profile (vertical exaggeration 63:1) as individual dots and the altitude of the spacecraft above the surface as a dashed line (Zuber et al., 2008). The other records, from top to bottom, show the observed r, θ, and ϕ components of the magnetic field in planetocentric coordinates and the total field magnitude, after calibration but prior to external field correction (Anderson et al., 2008). The unit for all magnetic field observations is nanoTesla (nT). One degree of longitude at the equator is approximately 43 km. Features at a, b, and c are discussed in the text. CA locates closest approach.

system (B_r positive outward, B_θ positive southward, B_ϕ positive eastward). The attitude uncertainty of the vector data is estimated at 0.1°, and instrument digitization resolution is 0.047 nT.

We use two approaches, one forward and one inverse, for the removal of external fields, as in Anderson et al. (2008). The forward model (TS04) is based on the adaptation of a terrestrial magnetospheric model for Mercury (Korth et al., 2004; Anderson et al., 2008), and the inverse approach (Anderson et al., 2008) involves the simultaneous estimation of the internal and external magnetic fields with a least squares, spherical harmonic expansion. The spherical harmonic solution parameterizes a magnetic field B into a part of internal origin B_{int} (sources internal to the observation altitude) and a part of external origin B_{ext}:

78
$$\begin{aligned} B &= B_{\text{int}} + B_{\text{ext}} \\ &= -\text{grad}\left[a\left\{\sum_{n,m}\left(g_{nm}\cos m\phi + h_{nm}\sin m\phi\right)\left(\frac{a}{r}\right)^{n+1} P_n^m(\cos\theta)\right\}\right] \\ &\quad -\text{grad}\left[a\left\{\sum_{n,m}\left(q_{nm}\cos m\phi + s_{nm}\sin m\phi\right)\left(\frac{r}{a}\right)^{n} P_n^m(\cos\theta)\right\}\right] \end{aligned}$$

Here (r, θ, ϕ) are spherical coordinates, a is Mercury's mean radius, $P_n^m(\cos\theta)$ are the Schmidt-normalized Legendre functions, (g_{nm}, h_{nm}) and (q_{nm}, s_{nm}) are expansion coefficients describing internal and external magnetic field contributions, respectively, and n and m are spherical harmonic degree and order. The selection of data for modeling of the internal field, and the identification of inbound and outbound bow shock and magnetopause crossing, follow Anderson et al. (2008).

All three closest approach (CA) locations were on the nightside. For Mariner 10 observations near CA used in this study, we currently have only Earth-based radar images (Harmon et al., 2007) to provide context. For the MESSENGER observations near CA, we have both radar images and a single laser altimeter profile (Zuber et al., 2008) to provide insight into the nature of the surface. Such information has proven to be important in understanding magnetic fields of crustal origin at Mars and the Moon (Langlais et al., 2004; Nicholas et al., 2007).

2.2. Laser altimeter observations

The Mercury Laser Altimeter (MLA) is a laser rangefinder operating at an 8 Hz rate. During MESSENGER's Mercury flyby, MLA collected a 3200-km long profile (Fig. 1), beginning about two minutes before CA and continuing for about ten minutes (Zuber et al., 2008). The topography exhibited a 5.2-km dynamic range along this profile, and several significant craters were sampled (Fig. 1), some of which are also seen in the radar images. Impact craters affect small-scale crustal magnetic fields through excavation of magnetic material, impact and thermal demagnetization, and subsequent remagnetization by thermal or shock processes in the presence of an ambient or core field (e.g., Lillis et al., 2008). Other geological processes (e.g., volcanism) can also affect prior magnetization.

3. Constraints on the presence of small-scale crustal magnetic fields

Small-scale crustal fields will be most easily identified near CA (Fig. 1) as features with wavelengths comparable to, or larger than, the distance of the spacecraft from the surface. At the MESSENGER CA altitude (201 km) this shortest wavelength on Mercury is ~5°. The decrease in |B| near CA, coincident with the deep crater "a" (Fig. 1), is interpreted not as a crustal magnetic feature but as a diamagnetic (plasma pressure) effect because it coincides with enhanced fluctuation amplitudes in the 1–10 Hz passband (Anderson et al., 2008) and with an increase in proton plasma count rates

Please cite this article as: Purucker, M.E., et al., Mercury's internal magnetic field: Constraints on large- and small-scale fields of crustal origin, Earth Planet. Sci. Lett. (2008), doi:10.1016/j.epsl.2008.12.017

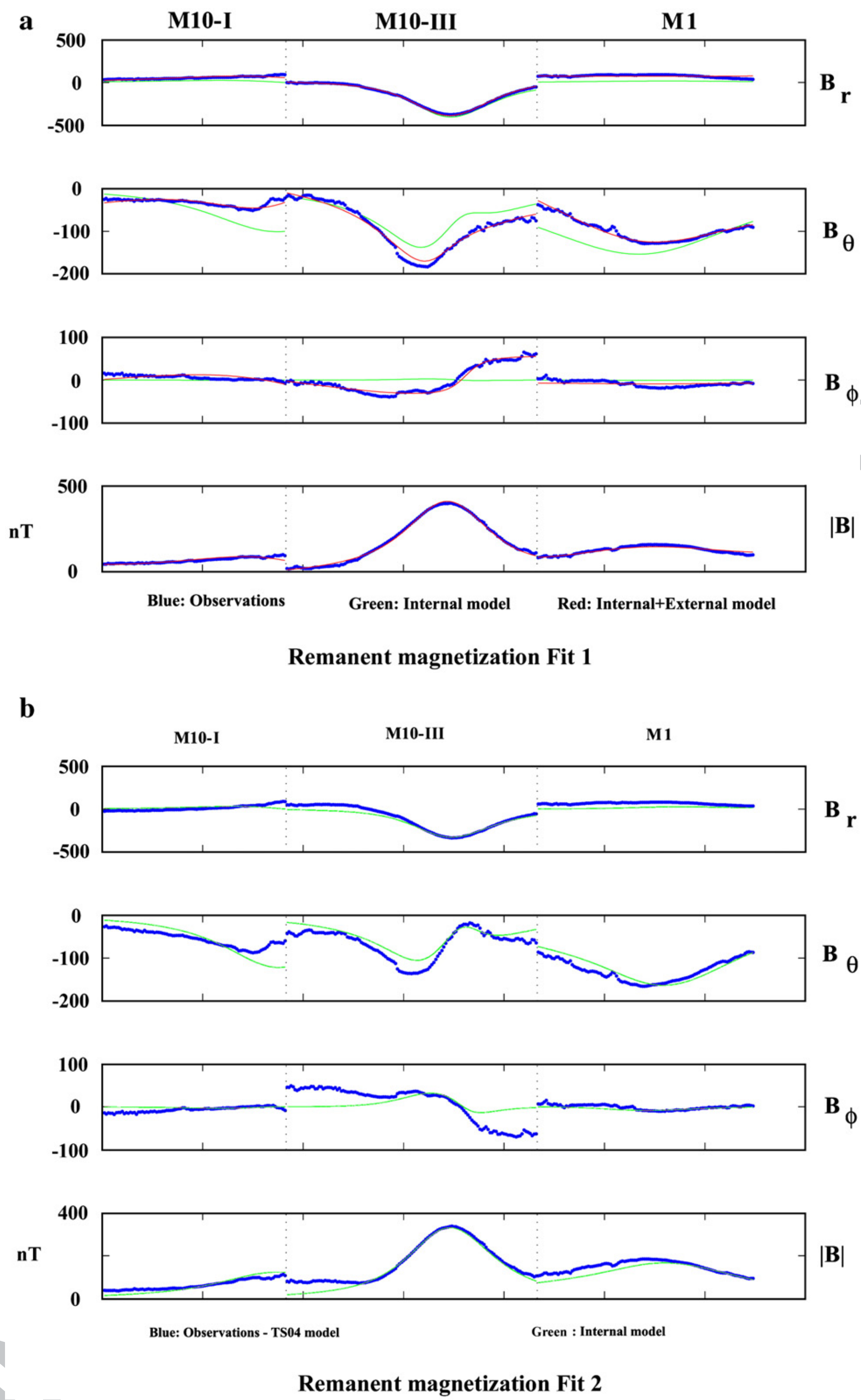

Fig. 2. Tests for the presence of large-scale crustal magnetic fields using data from all three flybys (M10-I is the first Mariner 10 flyby, M10-III is the third Mariner 10 flyby, and M1 is the first MESSENGER flyby). (a) Remanent magnetization fit 1. Observed magnetic field (blue) versus predictions (internal in green, internal+external in red) for laterally varying temperature and magnetized layer thickness (Aharonson et al., 2004). The solution includes co-estimates of the internal terms (g_{10}, g_{30}, and g_{32}, all other internal terms set to 0) and external terms (different for each flyby, and the $m=0$ terms are set to 0 since the flyby provides little latitudinal coverage). (b) Remanent magnetization fit 2. Observed magnetic field — TS04 external field model (Anderson et al., 2008) (in blue) versus predictions (in red) for same type of internal field model as in (a).

seen in the Fast Imaging Plasma Spectrometer observations (Zurbuchen et al., 2008). A smaller feature, “b” in Fig. 1, is less than 4 nT in magnitude, is not associated with either enhanced magnetic fluctuations or increased proton plasma count rates, and is not closely related to any surface feature seen by MLA. If the feature is of crustal origin, the relative strength of the ϕ component suggests that the spacecraft ground track passed near an edge of the source body. The prominent pair of craters seen at “c” has no magnetic field expression.

The Mariner 10 magnetometer observations made during the near-polar third flyby exhibit few features (Connerney and Ness, 1988) with the

Please cite this article as: Purucker, M.E., et al., Mercury's internal magnetic field: Constraints on large- and small-scale fields of crustal origin, Earth Planet. Sci. Lett. (2008), doi:10.1016/j.epsl.2008.12.017

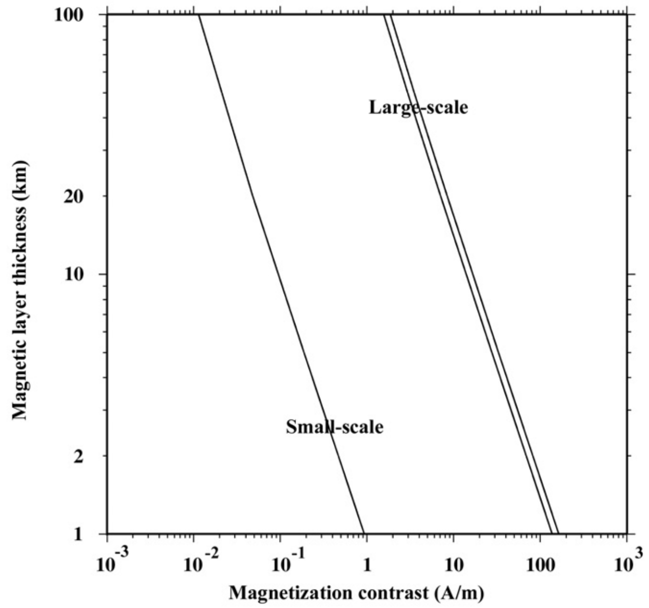

Fig. 3. Constraints on the product of thickness and magnetization contrast in Mercury's crust implied by the small-scale magnetic fields measured during the MESSENGER flyby and the large-scale fields measured during the third flyby of Mariner 10. The input to the small-scale calculation is the altitude of closest approach (201 km) and the maximum field that might be ascribed to small-scale crustal sources (the 4-nT feature associated with point "b" on Fig. 1). The input to the large-scale calculation is the altitude (352 km) of the maximum magnetic field magnitude (400.6 nT measured field, 338.1 nT after correction for external fields).

appropriate wavelengths (Fig. 2, M10-III). The equatorial pass of Mariner 10 (Fig. 2, M10-I) was affected by strong external field signatures close to CA.

Taken in total, these observations suggest that small-scale crustal magnetic fields, if they exist, are less than 4 nT at 201 km altitude. This limit is set by magnetic feature "b" in Fig. 1. The most basic question we would like to answer is the magnitude of the intensity of magnetization required to explain this result. By means of a constrained optimization approach, Parker (2003) showed how a series of bounds on the magnetic parameters of source regions may be determined with no assumptions on the direction of magnetization. These bounds can be derived from a single datum and solved in closed form with elementary functions. When $|B|$ has been measured, M_0 is the smallest possible scalar intensity of any distribution within a magnetic layer of thickness L bounded by the set of points with $h_1<z<h_2$, where z is the vertical Cartesian coordinate measured positive downward and the origin is at the measurement point:

$$M \geq M_0 = \frac{12|B|/\mu_0}{\left[6+\sqrt{3}\ln\left(2+\sqrt{3}\right)\ln(h_2/h_1)\right]}$$

and where μ_0 is the magnetic permeability of free space. Combining the distance from the planet with the 4-nT crustal field limit allows us to place constraints on the product of magnetization (A/m) and the magnetized layer thickness, as illustrated in Fig. 3. These calculations allow us to conclude, for example, that if the magnetization in this region is confined to a 10-km-thick layer, it must be coherently magnetized with an intensity of at least 0.1 A/m. Bounds can also be based on multiple observations, but Parker (2003) found that single-point bounds are not substantially inferior to those based on observation pairs.

4. Constraints on the presence of large-scale crustal magnetic fields

A constrained optimization approach can also be utilized to place bounds on the magnitude of large-scale crustal magnetic fields, if they originate as a consequence of variations in the thickness of a magnetized layer in Mercury's crust. The largest $|B|$ field was encountered on the third (polar) flyby of Mariner 10 (Fig. 2), where a field of 400.6 nT was measured at an altitude of 352 km above the planet at 66°N, 73°E. This value decreases to 338.1 nT if external fields are first removed with the TS04 model (Anderson et al., 2008). These bounds (Fig. 2), using the same one-datum formalism as before, imply that, if the magnetization is confined to a 50-km-thick layer, it must be at an intensity of at least 2.9 A/m. The flat-planet approximation used in this simplification can be shown to be quite accurate (Parker, 2003, Appendix A), with the largest errors at large layer thicknesses. These intensities are much stronger than those encountered on Earth; for example, newly magnetized basaltic rocks at a mid-ocean ridge may have a magnetization of 10 A/m, but the rocks with such magnetization are generally less than 1 km thick.

In the absence of local heterogeneities, it can be shown that variations in surface temperature (Vasavada et al., 1999) could control the depth to the base of a magnetized layer (Aharonson et al., 2004). These variations are a consequence of Mercury's spin-orbit coupling and result in insolation patterns that are symmetric about longitudes 0° and 90° and the equator. For Earth-like thermal gradients near the surface, the depth to the Curie temperature of any given magnetic carrier might vary by as much as 10 km. If a dynamo existed in Mercury at some time in the past, and if that dynamo field was approximately constant during cooling of the crust through the Curie temperature, we might expect to see a large-scale remanence in the crust that would produce an external field with a dominantly dipolar character (Fig. 4, remanent magnetization prediction). This result does not violate Runcorn's (1975) theorem, because lateral variations in shell thickness are a consequence of the variations in insolation.

Spherical harmonic expansions of the predicted large-scale variations in the thickness of the magnetic layer are dominated by the (n,m)=(2,0), (2,2), and (4,0) terms (Aharonson et al., 2004), which map to dominant (1,0), (3,0), and (3,2) terms in the magnetic Gauss coefficients. As a test of this theory, we can therefore solve a constrained least-squares problem for the internal Gauss field coefficients g_{10}, g_{30}, and g_{32}, using either the TS04 external field model or through co-estimation of internal and external fields (Figs. 2 and 4, and Table 1). These solutions do not reveal the predicted signal and yield much larger ratios of the dipole to the non-dipole terms than predicted by the remanent model. This outcome might imply that if remanence is the cause of Mercury's magnetic field, it is confined largely to the polar regions, and longitudinal variations are subordinate. However, the apparent absence of small-scale remanence features in the polar flyby observations of Mariner 10 makes this scenario unlikely. The model fit to the TS04-reduced model (Fig. 2-b and Table 1) leaves a significant residual field, especially in the horizontal component data over the poles, when compared with the other fits. Hence, the large-scale remanent model is unlikely to apply to Mercury, although limited coverage and the difficulty of separating internal from external fields make it difficult at this point to refute the model convincingly.

5. Discussion

Two more flybys will precede MESSENGER's entry into orbit about Mercury in 2011. The remaining flybys will be near-equatorial, like the first MESSENGER flyby, but will sample different longitudinal regions. In the subsequent orbital phase, the orbit will be highly elliptical, with periapsis near 60–72°N. The flybys will allow additional constraints to be placed on the presence of small-scale fields, and correlations will be possible among MLA-measured topographic profiles, features as seen on images, and any variations in internal magnetic field. The orbital phase should allow for detailed testing of the large-scale remanence idea.

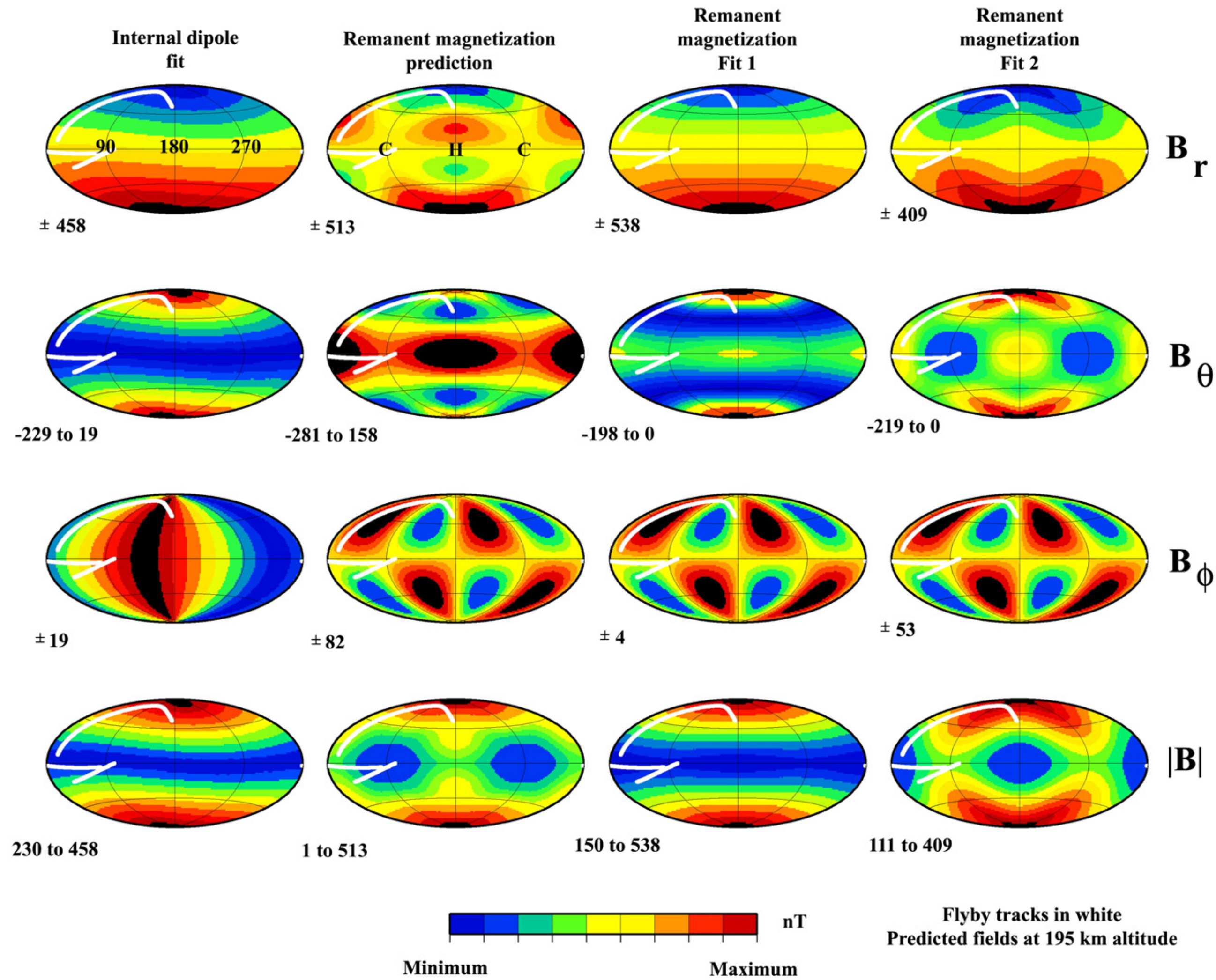

Fig. 4. Maps of predicted and fit vector and scalar magnetic fields expected for large-scale variations in magnetic layer thickness (right three columns) produced by laterally varying surface temperature fields, compared with maps of an internal dipole fit (left column). The cold (C) and hot (H) poles, corresponding to the thickest and thinnest portions of the magnetized layer, respectively, are shown on the radial field prediction map. These predictions are based on a 10-km thickness variation between cold and hot poles. Maps are centered on 180° longitude, and grid lines are every 90° in longitude and 45° in latitude. The maps show fields at an altitude of 195 km, and the location of the three flybys are shown as thick white lines. The color scale used in the maps is shown at the bottom. The mapping of the color scale to field values is different for each map and calculated using a histogram equalized approach. The numbers below and to the left of each map indicate the minimum and maximum magnetic fields present in that map. The statistics and spherical harmonic coefficients for each fit or prediction are shown in Table 1. Hammer projection.

It has long been recognized that magnetization within the terrestrial planets and Moon is controlled in part by the amount of available iron within the crust. Iron is partitioned among oxide, sulfide, and silicate phases in the crust (Clark, 1997), and only the first and perhaps the second of these phases can retain significant remanent magnetization in Mercury's environment. We can quantify a relationship between magnetization and iron content by using crustal iron abundances deduced from a variety of techniques and comparing these with the magnetization bounds deduced from the method of Parker (2003, Eq. 13) using satellite compilations of crustal magnetism. With the exception of Mercury, we have global coverage of the magnetic fields originating within the crust of these bodies. Magnetization values are minimum values, which are exceeded locally, and we select the largest measured field from the lowest altitude for determining magnetization bounds. On Mercury, we use the small-scale magnetization contrast for the reasons put forward in this paper. Increasing the altitude at which the magnetization bounds are calculated has the effect of reducing the bounds. At Mars, for example, the bound calculated with the 390-km-altitude mapping orbit of Mars Global Surveyor is 2.5 A/m, whereas the bound determined with the lower-altitude aerobraking orbit is 6.2 A/m.

For the average iron content of the terrestrial and lunar crusts we use the compilations of Lodders and Fegley (1998). At the Moon, the largest measured fields are over highland crust, so we select an Fe abundance typical of highland material. At Earth, the largest measured fields are over continental crust, so we select an Fe abundance typical of continental crustal composition. For Mercury we use the limits from the MESSENGER Neutron Spectrometer (NS) sensor, which provided an upper limit on surface Fe abundance from flyby observations (Solomon et al., 2008). For Mars we use values provided by the Gamma Ray Spectrometer (Hahn et al., 2007) on Mars Odyssey, which are in agreement with earlier constraints by McSween et al. (2003) from Martian meteorite chemistry, analysis of surface samples by Mars Pathfinder, spacecraft thermal emission spectra, and inferred crustal densities.

Crustal iron content and magnetization are compared in Fig. 5. Considering that both the small-scale magnetization constraint for

Please cite this article as: Purucker, M.E., et al., Mercury's internal magnetic field: Constraints on large- and small-scale fields of crustal origin, Earth Planet. Sci. Lett. (2008), doi:10.1016/j.epsl.2008.12.017

Mercury and the bound on iron abundance from NS observations are likely to decrease further with additional measurements, they are not inconsistent with a general relationship between crustal iron content and magnetization for the other terrestrial planetary bodies. Additional influences on magnetization include the strength of the dynamo field in which the magnetization was acquired and the mineralogy of the magnetic phases. We expect further insights into both topics once MESSENGER reaches orbit.

Differences between the magnetic properties of highland and mare materials on the Moon, and between oceanic and continental crust on Earth, highlight some of the other influences that should be considered in establishing relationships between crustal iron content and magnetization. For both the Moon and Earth, the crustal type with higher Fe abundance has lower measured magnetic fields (Maus et al., 2007; Purucker, 2008). For Earth, this outcome is the result of the significantly greater thickness of continental crust and because upward continuation of the fields produced by oceanic crust magnetized at alternating polarity tends to average out the effect of reversals. For the Moon, the lower fields over maria ~~is~~ likely the result of emplacement ages for mare units that postdate the time when there was a global lunar field.

6. Summary

We conclude that the case for large- and small-scale remanence on Mercury is weak, but further MESSENGER measurements are necessary to decide the issue unequivocally. Mercury appears to be consistent with a relationship between the amount of Fe in the crust and bounds on crustal magnetization observed for other terrestrial planets.

Acknowledgements

We thank Mario Acuña and two anonymous reviewers for a critical reading of the manuscript. Figures were produced using the GMT package of Wessel and Smith. The manuscript was written in coordination with that by Uno et al. (this ~~volume~~), and we thank Catherine Johnson for ongoing discussions and a review of an early draft of our paper. MP and TS were supported by the MESSENGER Participating Scientist grant NNH08CC05C. The MESSENGER project is supported by the NASA Discovery Program through contracts NASW-00002 with the Carnegie Institution of Washington and NAS5-97271 with the Johns Hopkins University Applied Physics Laboratory.

Table 1
Spherical harmonic coefficients and root mean square (RMS) misfits for fits and models shown in Figs. 2a, b and 4

	Internal dipole fit	Remanent magnetization prediction	Remanent magnetization fit 1	Remanent magnetization fit 2
g_{10}	−288.6	−85	−256.3	−229.5
g_{11}	15.3	–	–	–
h_{11}	19.2	–	–	–
g_{30}	–	−139	−48.2	−16.5
g_{32}	–	63	3.2	40.7
B_r RMS	14.2	–	12.2	42.8
B_θ RMS	17.2	–	6.6	18.5
B_ϕ RMS	7.5	–	6.3	22.7
~~Overall vector~~	13.6	–	8.8	29.9
~~Magnitude~~	9.5	–	5.2	13.3

Internal dipole fit is based on coestimating a common internal dipole and degree-2 external fields that differ for each flyby. Remanent magnetization prediction is based on the laterally varying temperature field of Aharonson et al. (2004). Remanent magnetization fit 1 is based on coestimating internal (g_{10}, g_{30}, and g_{32} only) and external fields (Figs. 2a and 4). Remanent magnetization fit 2 is based on removing the TS04 external field model (Anderson et al., 2008) prior to estimating the g_{10}, g_{30}, and g_{32} internal field coefficients (Figs. 2b and 4). ~~All values are in units of nT. The RMS misfits are shown as both vector misfits, and as misfits of the scalar field magnitude.~~

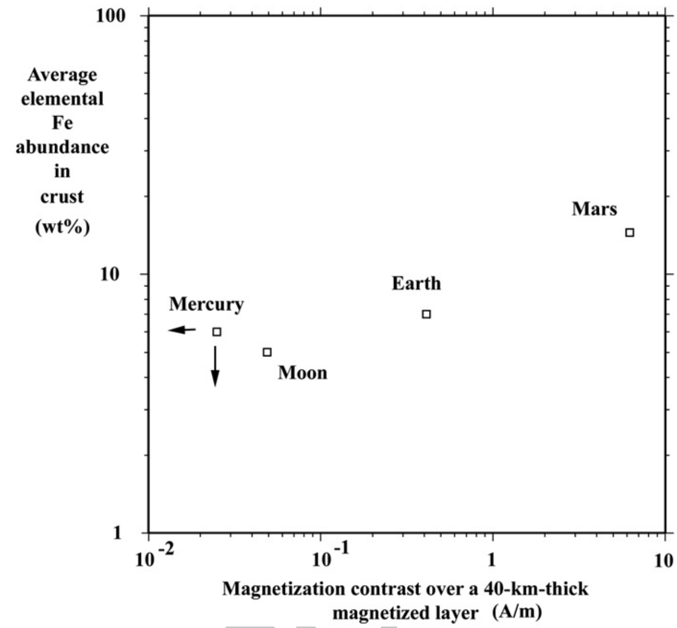

Fig. 5. Magnetization contrast (A/m) versus Fe content of crust (wt.%) for the terrestrial planets and Moon, for a 40-km-thick magnetic layer. Magnetization contrast is determined from satellite measurement by the use of Eq. (13) of Parker (2003). Individual altitude and field magnitude pairs are from Parker (2003) for Mars (at 131 km altitude), Nicholas et al. (2007) and Purucker (2008) for the Moon (at 18–30 km), Maus et al. (2007) for the Earth (at 350 km), and the small-scale magnetization contrast deduced for Mercury from this work. The Fe content of the near-surface crust is from compilations (Lodders and Fegley, 1998) for the Earth and Moon, from Hahn et al. (2007) and McSween et al. (2003) for Mars, and the upper limit from Solomon et al. (2008) for Mercury. The arrows on the Mercury symbol indicate that the Fe abundance, and perhaps the magnetization contrast, are bounds that may decrease with further measurements.

References

Aharonson, O., Zuber, M.T., Solomon, S.C., 2004. Crustal remanence in an internally magnetized non-uniform shell: a possible source for Mercury's magnetic field? Earth Planet. Sci. Lett. 218, 261–268.

Anderson, B.J., Acuña, M.H., Lohr, D.A., Scheifele, J., Raval, A., Korth, H., Slavin, J.A., 2007. The magnetometer instrument on MESSENGER. Space Sci. Rev. 131, 417–450.

Anderson, B.J., Acuña, M.H., Korth, H., Purucker, M.E., Johnson, C.L., Slavin, J.A., Solomon, S.C., McNutt, R.L., 2008. The structure of Mercury's magnetic field from MESSENGER's first flyby. Science 321, 82–85.

Clark, D.A., 1997. Magnetic petrophysics and magnetic petrology: aids to geological interpretation of magnetic surveys. AGSO J. Aust. Geol. Geophys. 17, 83–103.

Connerney, J.E.P., Ness, N.F., 1988. Mercury's magnetic field and interior. In: Vilas, F., Chapman, C.R., Matthews, M.S. (Eds.), Mercury. University of Arizona Press, Tucson, Ariz., pp. 494–513.

Hahn, B.C., McLennan, S.M., Taylor, G.J., Boynton, W.V., Dohn, J.M., Finch, M.J., Hamara, D.K., Janes, D.M., Karunatillake, S., Keller, J.M., Kerry, K.E., Metzger, A.E., Williams, R.M.S., 2007. Mars Odyssey gamma ray spectrometer elemental abundances and apparent relative surface age: implications for Martian crustal evolution. J. Geophys. Res. 112, E03S11. doi:10.1029/2006JE002821.

Harmon, J.K., Slade, M.A., Butler, B.J., Head III, J.W., Rice, M.S., Campbell, D.B., 2007. Mercury: radar images of the equatorial and midlatitude zones. Icarus 187, 374–405.

Korth, H., Anderson, B.J., Acuña, M.H., Slavin, J.A., Tsyganenko, N.A., Solomon, S.C., McNutt Jr., R.L., 2004. Determination of the properties of Mercury's magnetic field by the MESSENGER mission. Planet. Space Sci. 52, 733–746.

Langlais, B., Purucker, M., Mandea, M., 2004. Mars crustal magnetic fields. J. Geophys. Res. 109, E02008. doi:10.1029/2003JE002048.

Lillis, R.L., Frey, H.V., Manga, M., Mitchell, D.L., Lin, R.P., Acuña, M.H., Bougher, S.W., 2008. An improved crustal magnetic map of Mars from electron reflectometry: highland volcano magmatic history and the end of the Martian dynamo. Icarus 194, 575–596.

Lodders, K., Fegley, B., Jr., 1998. The Planetary Scientist's Companion, Oxford University Press, New York, pp. 124, 140, and 177.

Maus, S., Lühr, H., Rother, M., Hemant, K., Balasis, G., Ritter, P., Stolle, C., 2007. Fifth generation lithospheric magnetic field model from CHAMP satellite measurements. Geochem. Geophys. Geosyst. 8, Q05013. doi:10.1029/2006GC001521.

McSween Jr., H.Y., Grove, T.L., Wyatt, M.B., 2003. Constraints on the composition and petrogenesis of the Martian crust. J. Geophys. Res. 108 (E12), 5135. doi:10.1029/2003JE002175.

Merrill, R.T., 1981. Toward a better theory of thermal remanent magnetization. J. Geophys. Res. 86, 937–949.

Nicholas, J.B., Purucker, M.E., Sabaka, T.J., 2007. Age spot or youthful marking: origin of Reiner Gamma. Geophys. Res. Lett. 34, L02205. doi:10.1029/2006GL027794.

Parker, R.L., 2003. Ideal bodies for Mars magnetics. J. Geophys. Res. 108 (E1), 5006. doi:10.1029/2001JE001760.

Purucker, M.E., 2008. A global model of the internal magnetic field of the Moon based on Lunar Prospector magnetometer observations. Icarus 197, 19–23.

Runcorn, S.K., 1975. An ancient lunar magnetic dipole field. Nature 253, 701–703.

Solomon, S.C., McNutt Jr., R.L., Watters, T.R., Lawrence, D.J., Feldman, W.C., Head, J.W., Krimigis, S.M., Murchie, S.L., Phillips, R.J., Slavin, J.A., Zuber, M.T., 2008. Return to Mercury: a global perspective on MESSENGER's first Mercury flyby. Science 321, 59–62.

Stephenson, A., 1976. Crustal remanence and the magnetic moment of Mercury. Earth Planet. Sci. Lett. 28, 454–458.

Trávníček, P., Hellinger, P., Schriver, D., 2007. Structure of Mercury's magnetosphere for different pressure of the solar wind: three dimensional hybrid simulations. Geophys. Res. Lett. 34, L05104. doi:10.1029/2006GL028518.

Uno, H., Johnson, C.L., Anderson, B.J., Korth, J., Solomon, S.C., 2008. Modeling Mercury's internal magnetic field using smooth inversions. Earth Planet. Sci. Lett. This issue. Q1

Vasavada, A.R., Paige, D.A., Wood, S.E., 1999. Surface temperatures on Mercury and the Moon and the stability of polar ice deposits. Icarus 141, 179–193.

Zuber, M.T., Aharonson, O., Aurnou, J.M., Cheng, A.F., Hauck II, S.A., Heimpel, M.H., Neumann, G.A., Peale, S.J., Phillips, R.J., Smith, D.E., Solomon, S.C., Stanley, S., 2007. The geophysics of Mercury: current status and anticipated insights from the MESSENGER mission. Space Sci. Rev. 131, 105–132.

Zuber, M.T., Smith, D.E., Solomon, S.C., Phillips, R.J., Peale, S.J., Head III, J.W., Hauck II, S.A., McNutt Jr., R.L., Oberst, J., Neumann, G.A., Lemoine, F.G., Sun, X., Barnouin-Jha, O., Harmon, J.K., 2008. Laser altimeter observations from MESSENGER's first Mercury flyby. Science 321, 77–79.

Zurbuchen, T.H., Raines, J.M., Gloeckler, G., Krimigis, S.M., Slavin, J.A., Koehn, P.L., Killen, R.M., Sprague, A.L., McNutt Jr., R.L., Solomon, S.C., 2008. MESSENGER observations of the composition of Mercury's ionized exosphere and plasma environment. Science 321, 90–91.

Please cite this article as: Purucker, M.E., et al., Mercury's internal magnetic field: Constraints on large- and small-scale fields of crustal origin, Earth Planet. Sci. Lett. (2008), doi:10.1016/j.epsl.2008.12.017